



Tuning the emission property of carbazole-caped cyclometalated platinum(II) complexes and its application for enhanced luminescent oxygen sensing

Wanhua Wu, Wenting Wu, Shaomin Ji, Huimin Guo, Jianzhang Zhao*

State Key Laboratory of Fine Chemicals, School of Chemical Engineering, Dalian University of Technology, 2 LingGong Road, Dalian 116024, PR China

ARTICLE INFO

Article history:

Received 9 November 2010

Received in revised form

28 February 2011

Accepted 1 March 2011

Keywords:

Cyclometalated complex

Platinum

Oxygen sensing

Phosphorescence

Triplet state

Carbazole

ABSTRACT

Carbazole-caped cyclometalated platinum(II) complexes aryl-*R*-ppyPt(acac) (where *ppy* = 4-phenylpyridine, acac = acetylacetonato, aryl = carbazole and *R* is linker) were synthesized. The carbazole group is attached to the *ppy* ligand via α -diketo moiety (**Pt-1**) and (**Pt-2**) or C–C single bond (**Pt-3**), by Sonogashira or Negishi coupling reactions. We found that the ethynylene bonds of the C^N ligands were oxidized to α -diketo or methylene-keto structure during the metalation with K₂PtCl₄. Emissions beyond 550 nm were observed for **Pt-1**, with electron-withdrawing α -diketo moiety attached to *ppy* ligand, compared to the emission at 486 nm for the parent complex *ppy*Pt(acac). Extended phosphorescence lifetime ($\tau_p = 12.4 \mu\text{s}$) and enhanced phosphorescence quantum yield ($\Phi_p = 66\%$) were observed for **Pt-3** compared to *ppy*Pt(acac) ($\tau_p = 2.4 \mu\text{s}$ and $\Phi_p = 15\%$), we attribute the enhanced phosphorescence property to the electron-donating carbazole substituent. With density functional theoretical calculations (DFT), we found that the carbazole moiety is involved in the HOMO (**Pt-3**), the α -diketo moiety is involved in the LUMO (**Pt-1**), thus the energy gaps between the HOMO and LUMO in both cases were decreased and red-shifted emission is expected, compared to *ppy*Pt(acac). The different emission properties of 1,2-dione containing complexes (**Pt-1** and **Pt-2**) and the **Pt-3** were rationalized by the spin density surface analysis of the complexes. The luminescent O₂ sensing properties of these complexes were studied in solution and in polymer films, for which fast response time (3.3 s) and recovery time (3.7 s) were observed. Two-site model fitting indicated that complex **Pt-3** is the most sensitive O₂ sensing material among the complexes studied herein, with quenching constant of $K_{SV} = 0.0238 \text{ Torr}^{-1}$.

© 2011 Elsevier B.V. All rights reserved.

1. Introduction

Recently cyclometalated Pt(II) complexes, such as *ppy*Pt(acac) (*ppy* = 2-phenylpyridine, acac = acetylacetonato), attracted much attention due to their applications in organic light emitting diodes (OLED) [1–4], luminescent molecular sensors [5–7] and for their photophysical properties [8–10]. These complexes show strong triplet emission in fluid solution at room temperature, due to the spin-orbit coupling effect of the heavy atom, which leads to the population of ³MLCT/³IL emissive excited states of the complexes upon photoexcitation. Typical cyclometalated Pt(II) complexes give relatively short emission wavelength, e.g. at ca. 500 nm. Thus, tuning the emission color is critical for electroluminescent materials. However, it is still a challenge to tune the emission color of the Pt(II) complexes and we noticed that the π -conjugation framework of the typical *ppy* ligands has never been extended by ethynylene groups, to tune the emission wavelength of the complexes.

* Corresponding author. Tel./fax: +86 (0)411 8498 6236.

E-mail address: zhaojzh@dlut.edu.cn (J. Zhao).

On the other hand, luminescent oxygen sensing is attracting much attention due to its applications in biological, environmental, chemical and clinical science [1,2]. Proper selection of phosphorescent dye is pivotal for luminescent O₂ sensing. Currently, the dyes for O₂ sensing include polypyridine Ru(II) complexes, Pt(II)/Pd(II) porphyrin complexes and more recently the cyclometalated complexes [1,2]. We noticed that the *ppy*Pt(acac) complexes show phosphorescent lifetime in the range of microseconds (μs), which are ideal for oxygen sensing [2]. To the best of our knowledge, however, no systematic study has been carried out on the luminescent O₂ sensing properties of the cyclometalated Pt(II) complexes [11–19].

Recently we have been interested in synthesis of phosphorescent metal complexes and studying the photophysical properties and exploring their applications, such as in luminescent oxygen sensing [20–25]. We and others found that the luminescent lifetimes of the Ru(II) bispyridine complexes can be significantly tuned by ligand modification (introduce of new triplet excited states) [20–28]. We anticipate that the emission wavelength and phosphorescence lifetime of the cyclometalated Pt(II)(acac) complexes may probably be

tuned by the similar approach of ligand modification, thus we set out to prepare new cyclometalated Pt(II) complexes to modulate the photophysical properties and to explore the application of these complexes for luminescent O₂ sensing.

The design rationales for the complexes are to extend the π -conjugation framework of the *ppy* ligands by ethynylene groups (–C≡C–). Carbazole was selected to attach to the phenyl moiety of the *ppy* ligand to shift the emission wavelength to the red end of the spectrum [3]. Thus we prepared new cyclometalated Pt complexes with carbazole substituted *ppy* ligand and ethynylene group was used as linker between the carbazole and the *ppy* ligand (Scheme 1). We found that the ethynyl ligand was oxidized to keto structure during the metalation of the ligands with K₂PtCl₄. All the complexes show intensive room temperature phosphorescence in fluid solution. Red-shifted emission wavelength was found for the complexes (ca. 550 nm), compared to the parent complex *ppy*Pt(acac) (486 nm). Greatly improved phosphorescence property were found for **Pt-3** compared to the parent complex *ppy*Pt(acac). The luminescent O₂ sensing properties of these complexes in polymer films were also studied. Our systematic study on the photophysical properties and the O₂ sensing properties of the cyclometalated Pt(II) complexes may prove useful for future development of the phosphorescent cyclometalated Pt(II) complexes.

2. Results and discussions

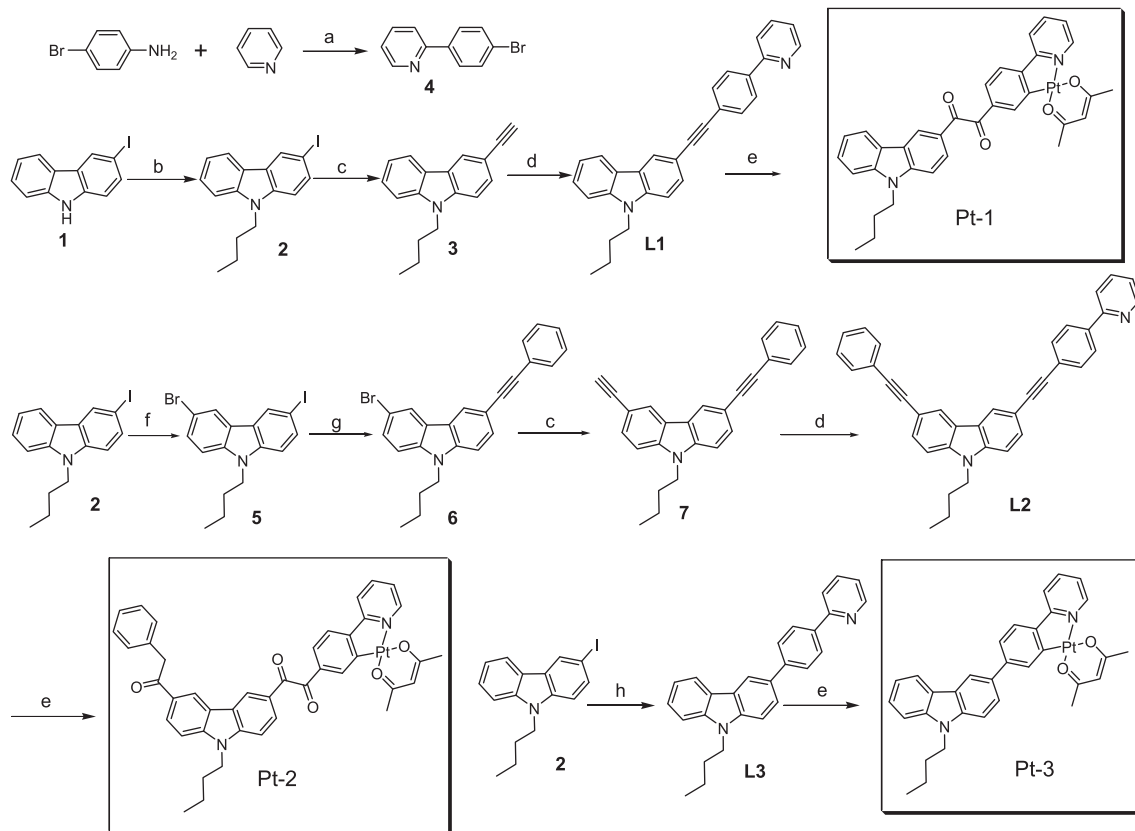
2.1. Synthesis

The design rationale of the ligand lies on the notion that by attachment of an electron pushing group to the *ppy* ligand will

strengthen the ligand field of the *ppy* moiety, thus improve luminescence properties, such as prolonged phosphorescence lifetime and higher phosphorescence quantum yields could be expected [3]. Furthermore, the electron-donating appendents on the phenyl subunit of the *ppy* ligand may rise the energy level of the highest occupied molecular orbitals (HOMO) of the cyclometalated Pt complex, but the energy level of the lowest unoccupied molecular orbital (LUMO) is unaffected, as a result the decreased HOMO–LUMO energy gap leads to red-shifted emission, compared to the parent complex of *ppy*Pt(acac) ($\lambda_{em} = 486$ nm) [3].

4'-bromo-*ppy* was obtained by a feasible approach [29]. The bromo substitution at *ppy* allows further derivatization of the ligand, such as with Sonogashira or Negishi coupling reactions (Scheme 1). *N*-butyl ethynylated carbazole was prepared and reacted with 4'-bromo-*ppy* via the Sonogashira coupling reaction. We prepared ligand **L2** with the 3-iodo-6-bromo carbazole. Reaction of K₂PtCl₄ with HC^{*N*} ligand precursor (substituted *ppy*) forms the chloride-bridged dimer, C^{*N*}Pt(μ -Cl)₂PtC^{*N*}, which is then cleaved with acetyl acetone to give the corresponding monomeric C^{*N*}Pt(O^{*O*}) complex.

For **Pt-1** and **Pt-2**, however, the desired ethynyl structures were not obtained. Instead, the products were proved to be the α -diketo structure (Scheme 1). This is proved by the ¹³C NMR data (185.72 ppm, 184.23 ppm for **Pt-1** and 196.53, 196.38, 195.38, 43.24 for **Pt-2**, respectively). Further evidence is from the high resolution mass spectra, for which $m/z = 725.1911$ and 843.0262 were observed for the **Pt-1** and **Pt-2**, respectively. This is due to the Pt catalyzed oxidation reaction during the metalation procedure of the ethynyl ligand with K₂PtCl₄ [30]. For **Pt-2**, gCOSY, TOCSY and gHMBC spectra were also measured to validate the proposed molecular structures (see Figs. S16–S18 in Supporting information).



Scheme 1. Synthesis of the cyclometalated Pt(II) complexes **Pt-1**, **Pt-2** and **Pt-3**. (a) NaNO₂/HCl, NaCO₃; (b) BuBr, NaH, r.t.; (c) trimethylsilylacetylene, Pd(PPh₃)₂Cl₂, PPh₃, CuI, NEt₃, reflux; K₂CO₃/methanol; (d) **4**, Pd(PPh₃)₄, CuI, toluene/(*i*-Pr)₂NH, reflux; (e) i: K₂PtCl₄, ethoxyethanol/water, ii: Hacac, Na₂CO₃, ethoxyethanol; (f) NBS, r.t.; (g) 1-ethynylbenzene, Pd(PPh₃)₄, CuI; (h) **4**, *n*-BuLi, ZnCl₂, 78 °C.

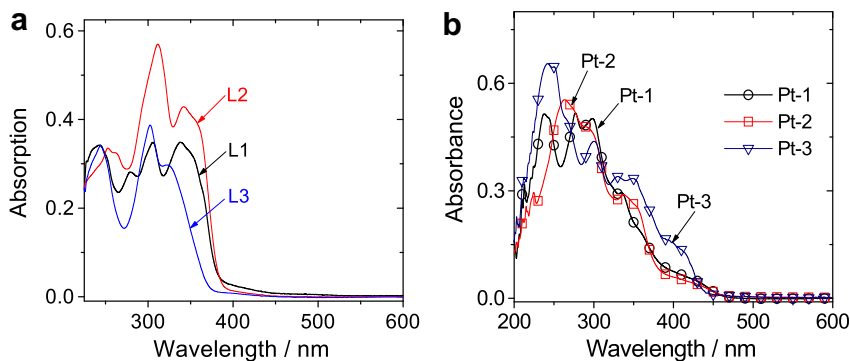


Fig. 1. UV–vis absorption of (a) the ligands and (b) the complexes. 1.0×10^{-5} mol dm $^{-3}$ in CH $_2$ Cl $_2$, 20 °C.

2.2. UV–vis absorption of the ligands and the cyclometalated Pt complexes

The absorption bands of ligand **L3** were below 370 nm (Fig. 1a). These absorptions were assigned to the transitions involving the carbazole related π -conjugation system. The relatively red-shifted absorptions of **L1** and **L2** are due to the extended π -conjugation of the ligand.

Compared to the free ligands, the complexes show red-shifted absorption (Fig. 1b). The new weak absorption at 420 nm with molar extinction coefficients in the range of 0.473 – 1.01×10^4 cm $^{-1}$ mol $^{-1}$ dm 3 , are due to the allowed $S_0 \rightarrow {}^1$ MLCT and the $S_0 \rightarrow {}^1$ ILCT transitions [3,31]. The absorptions below 350 nm are due to the π - π^* transition of the C \wedge N fragment.

2.3. Emission of the ligands and the Pt complexes

The emissions of the ligands and complexes were studied (Fig. 2). The emission of the ligands is in agreement with the extent of the π -conjugation of the ligands. For example, **L2** shows the largest π -conjugation framework, correspondingly, this ligand shows the longest emission wavelength. The opposite was observed for **L3** [32].

With metalation, **Pt-3** shows red-shifted emission at 540 nm, which is due to the 3 MLCT/ 3 ILCT transitions of the C \wedge N Pt (acac) compounds [3,31]. Note the emission wavelength is red-shifted by about 54 nm compared to *ppy*Pt(acac) ($\lambda_{em} = 486$ nm) [31]. The red-shifted emission can be rationalized by the attachment of the electron-donating carbazole moiety to the phenyl group of the *ppy*

ligand, where the HOMO is localized [3,31,33]. As a result, the energy level of the HOMO will increase, but the energy level of the LUMO is unaffected. Thus decreased HOMO-LUMO energy gap is resulted and red-shifted emission will be expected [3,31,34].

Notably, **Pt-3** shows much longer phosphorescence lifetime ($\tau_p = 12.4$ μ s) and much higher phosphorescence quantum yield ($\Phi_p = 66\%$) than *ppy*Pt(acac), which gives $\tau_p = 2.6$ μ s and $\Phi_p = 15\%$, respectively [31]. We attribute the enhanced phosphorescence of **Pt-3** to the strengthened ligand field, due to the electron-donating carbazole moiety. Thus the non-radiative decay channel of 3 MC state will be elevated to be much higher above the emissive 3 MLCT/ 3 IL state [3]. Previously Ir(III) complexes with the carbazole moiety directly cyclometalated were reported, but those Ir(III) complexes show much shorter phosphorescence lifetimes and much lower quantum yields [6].

We demonstrate that direct metalation of the carbazole moiety is not necessary for long emission wavelength, thus more diverse chromophores could be used in preparation of the complexes which give red-shifted emission, vs. *ppy*Pt(acac) [3,31,35]. This emission wavelength tuning strategy for the cyclometalated Pt(II) (acac) complex may prove significant for development of novel electroluminescent materials. It should be pointed out that triplet emitter **Pt-3** is multifunctional, as carbazole moiety is incorporated in the complexes, which is known as a good hole transporter [34,35], thus this complex could be used as OLED material.

Interestingly, different emission profiles were observed for complexes **Pt-1** and **Pt-2**. The emission bands at 554 nm and 556 nm are not well-resolved, which is different from that of **Pt-3** (Fig. 2). Furthermore, initially we suppose that **Pt-1** and **Pt-2** will

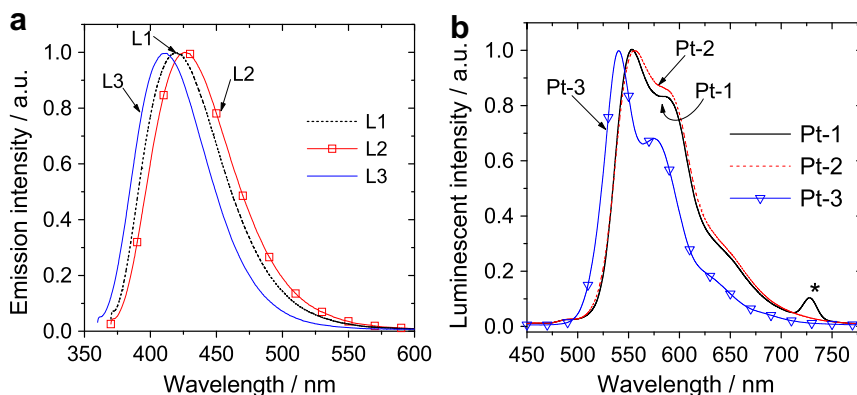


Fig. 2. Emission spectra of the ligands and the Pt(II) complexes. The emission intensity of the complexes is not comparable. 1.0×10^{-5} mol dm $^{-3}$ in CH $_2$ Cl $_2$, r. t. (a) **L1**: $\lambda_{ex} = 370$ nm, **L2**: $\lambda_{ex} = 360$ nm, **L3**: $\lambda_{ex} = 350$ nm. (b) **Pt-1**: $\lambda_{ex} = 370$ nm, **Pt-2**: $\lambda_{ex} = 364$ nm, **Pt-3**: $\lambda_{ex} = 350$ nm. The asterisk (*) in b indicates the second order transition of the monochromator of the fluorescence spectrometer.

Table 1
Photophysical properties of the ligands and the Pt(II) complexes.

| Compounds | $\lambda_{\text{abs}}/\text{nm}^{\text{a}}$ | $\epsilon/10^4 \text{ cm}^{-1} \text{ mol}^{-1} \text{ dm}^3$ | Emission | | | |
|-----------------|---|---|----------------------------------|---------------------|-------------------|--------------------------|
| | | | $\lambda_{\text{em}}^{\text{a}}$ | τ | ϕ | I_0/I_{100}^{d} |
| Ligand 1 | 305/338 | 3.48/3.38 | 426 | 1.38 ns | 0.75 ^b | 1.2 |
| Ligand 2 | 311/342 | 5.71/4.29 | 422 | 3.16 ns | 0.56 ^b | 1.3 |
| Ligand 3 | 302/323 | 3.88/2.97 | 410 | 1.77 ns | 0.62 ^b | 1.2 |
| Pt-1 | 277/298/335 | 5.18/5.02/2.95 | 554 | 1.86 μs | 0.13 ^c | 10.1 |
| Pt-2 | 264/292/337 | 5.54/4.74/2.90 | 556 | 2.82 μs | 0.20 ^c | 11.6 |
| Pt-3 | 300/331/348 | 4.10/3.12/3.06 | 540 | 12.40 μs | 0.66 ^c | 71.1 |

^a Result of compound in deaerated DCM solution ($1.0 \times 10^{-5} \text{ mol dm}^{-3}$). In solution of CH_2Cl_2 , 298 K.

^b Result of deaerated solution, with compound quinone as the standard ($\phi = 0.547$ in 0.05 M sulphuric acid).

^c Result of deaerated solution, with complex $\text{Pt}(\text{tBu}_2\text{bpy})(\text{C}\equiv\text{C}-\text{Ph})_2$ ($\phi = 0.496$ in MeCN) as the standard.

^d I_0 is the emission intensity under N_2 atmosphere and I_{100} is the emission intensity under O_2 atmosphere.

show blue-shifted emission, due to the electron-withdrawing diketo moiety on the phenyl group of the *ppy* ligand, where HOMO is localized [31]. To our surprise, **Pt-1** and **Pt-2** show red-shifted emission compared to *ppyPt(acac)* ($\lambda_{\text{em}} = 486 \text{ nm}$). The emission wavelength of **Pt-1** and **Pt-2** are even longer than the emission of **Pt-3**. This observation is in stark contrast to the accepted knowledge that *ppyPt(acac)* complex will show blue shift emission given that an electron-withdrawal moiety is attached to the phenyl group of the *ppy* ligand [3,31,34]. As the α -diketo is electron-withdrawal, thus we propose the diketo moiety in **Pt-1** and **Pt-2** may be involved in the LUMO orbit and acts as an electron sink, i.e. the electronic structure of the emissive state may be different from the typical ${}^3\text{MLCT}/{}^3\text{IL}$ excited state of the normal *ppyPt(acac)* complexes, featured with phenyl \rightarrow pyridine charge transfer [3,31]. The LUMO of the complexes **Pt-1** and **Pt-2** will be stabilized with this electron-withdrawal moiety thus the energy gap of the HOMO-LUMO may be decreased, as a result, the emission may show bathochromic shift compared to *ppyPt(acac)* [21–25].

The emission intensity of the complexes can be significantly quenched by O_2 . This result also supports the triplet nature of the emissions, as well as long phosphorescence lifetimes. Our strategy of using an electron sink to perturb the electronic structure of the T_1 excited state to tune the emission property may prove useful for preparation of new cyclometalated Pt complexes as electroluminescent materials. The electron-withdrawal diketo moiety may serve as the electron-transporting moiety for these multifunctional materials. Furthermore, the use of electron-donating carbazole to increase the phosphorescence quantum yield and prolong the phosphorescence lifetime is useful for design of new phosphorescent cyclometalated complexes.

The photophysical parameters of the ligands and the cyclometalated Pt(II) complexes were compiled in Table 1. For the

emission bands in the range of 500 nm–700 nm (the phosphorescence emission band), the phosphorescent lifetime is in the range of 1.86 μs –12.4 μs .

2.4. DFT/TDDFT calculation of the complexes: the electronic structure of the low-lying excited states

Recently DFT methods have been used to study the photophysical properties of the singlet and triplet emitters [20,36–40]. The photophysics of luminophores can be better understood by revealing the molecular orbitals of the electronic transitions of the luminophore, this is beneficial for the future design of luminophores with predetermined photophysical properties [20,40].

Firstly **Pt-3** was studied with the DFT calculations. The dihedral angle between the carbazole moiety and the *ppy* moiety was observed as 37° for the optimized ground state geometry (Fig. 3). The optimized bond length are Pt–N (2.024 Å), Pt–C (1.986 Å) and Pt–O (2.04–2.15 Å), respectively. The bond angles of C–Pt–N (81.2°) and O–Pt–O (90.6°), are in good agreement with the single crystal structure of the related cyclometalated Pt complexes [31].

We found the electron-rich carbazole moiety contributes significantly to the HOMO, while the LUMO is predominantly localized on the pyridine/phenyl groups of the *ppy* ligand (Fig. 3). The Pt atom contributes slightly to the MOs. These MOs can be used to rationalize the red-shifted emission of the complexes compared to the parent complex *ppyPt(acac)*. The energy level of HOMO will be increased with the electron-donating carbazole fragment appended at the phenyl group of the *ppy* ligand (-5.06 eV), vs. the HOMO energy of -5.42 eV for *ppyPt(acac)*. Both **Pt-3** and *ppyPt(acac)* share similar LUMO energy level of -1.55 eV and -1.58 eV , respectively. Thus the energy gap between HOMO

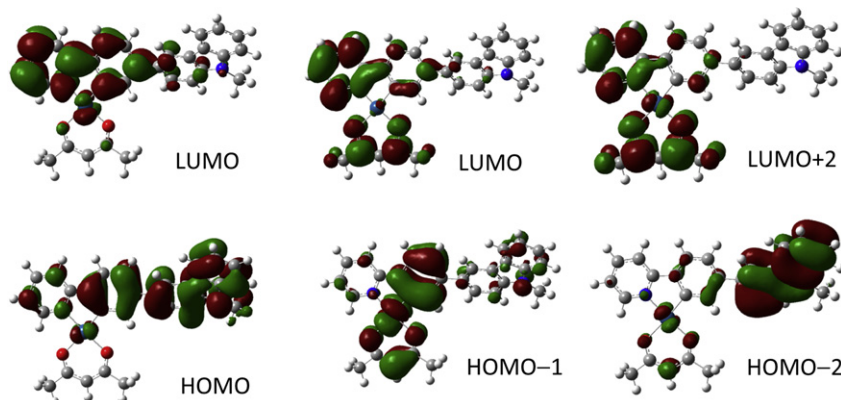


Fig. 3. Frontier molecular orbitals for **Pt-3**, calculated by DFT/TDDFT at the B3LYP/6-31G(d)/LanL2DZ level using Gaussian 09.

Table 2

Electronic excitation energies (eV) and corresponding Oscillator strengths (f), main configurations and CI coefficients of the Low-lying electronically excited states of complex **Pt-3**, calculated by TDDFT//B3LYP/6-31G(d)/LanL2DZ, based on the DFT//B3LYP/6-31G(d)/LanL2DZ Optimized ground state geometries.

| Electronic transition | TDDFT//T//B3LYP/6-31G(d) | | | | |
|-----------------------|--------------------------|---------------------|--------------------------|-----------------|------------|
| | Energy ^a | f^b | Composition ^c | CI ^d | Character |
| S0 → S1 | 3.03 eV/ 409 nm | 0.2209 | H → L | 0.5588 | ILCT |
| | | | H-3 → L | 0.1817 | LLCT, MLCT |
| | | | H-1 → L | 0.3279 | LLCT, MLCT |
| S0 → S2 | 3.24 eV/ 383 nm | 0.1953 | H-1 → L | 0.5753 | LLCT, MLCT |
| | | | H → L | 0.3618 | ILCT |
| S0 → S3 | 3.47 eV/ 357 nm | 0.0050 | H-4 → L | 0.6924 | MLCT |
| S0 → S6 | 3.68 eV/ 336 nm | 0.1413 | H-3 → L | 0.3660 | LLCT, MLCT |
| | | | H-2 → L | 0.2603 | ILCT |
| | | | H-1 → L | 0.1099 | LLCT, MLCT |
| | | | H-1 → L+1 | 0.2088 | MLCT, ILCT |
| | | | H → L+1 | 0.4244 | LLCT, ILCT |
| | | | H → L+3 | 0.1552 | ILCT, MLCT |
| | | | H-5 → L | 0.1774 | ILCT, LLCT |
| S0 → T1 | 2.47 eV/ 502 nm | 0.0000 ^e | H-3 → L | 0.2280 | LLCT, MLCT |
| | | | H-2 → L | 0.1252 | ILCT |
| | | | H-1 → L | 0.2460 | LLCT, MLCT |
| | | | H → L | 0.5847 | ILCT |
| | | | H → L+1 | 0.1321 | ILCT |

^a Only the selected low-lying excited states are presented.

^b Oscillator strength.

^c H stands for HOMO and L stands for LUMO. Only the main configurations are presented.

^d The CI coefficients are in absolute values.

^e No spin-orbital coupling effect was considered, thus the f values are zero.

Table 3

Electronic excitation energies (eV) and corresponding oscillator strengths (f), main configurations and CI coefficients of the Low-lying Electronically excited states of complex **Pt-1**, Calculated by TDDFT//B3LYP/6-31G(d)/LanL2DZ, based on the optimized ground state geometries.

| Electronic transition | TDDFT//B3LYP/6-31G(d) | | | | |
|-----------------------|-----------------------|---------------------|--------------------------|-----------------|-----------|
| | Energy ^a | f^b | Composition ^c | CI ^d | Character |
| S0 → S1 | 2.73 eV/ 455 nm | 0.0020 | H-5 → L | 0.1108 | MLCT |
| | | | H-4 → L | 0.4079 | MLCT |
| | | | H-4 → L+1 | 0.1751 | ILCT |
| S0 → S2 | 2.85 eV/ 435 nm | 0.0502 | H-2 → L | 0.4048 | ILCT |
| | | | H-3 → L | 0.1627 | LLCT |
| | | | H-2 → L | 0.1331 | ILCT |
| S0 → S10 | 3.76 eV/ 330 nm | 0.1360 | H → L | 0.6098 | MLCT |
| | | | H-6 → L | 0.1879 | LLCT |
| | | | H-2 → L+1 | 0.1661 | ILCT |
| | | | H-1 → L+1 | 0.5234 | ILCT |
| S0 → T1 | 2.27 eV/ 545 nm | 0.0000 ^e | H → L+2 | 0.2556 | LLCT |
| | | | H-3 → L+2 | 0.4316 | LLCT |
| | | | H-5 → L | 0.1383 | MLCT |
| | | | H-4 → L | 0.3863 | ILCT |
| | | | H-4 → L+1 | 0.2242 | MLCT |
| | | | H-2 → L | 0.4391 | ILCT |
| | | | H-2 → L+1 | 0.2119 | ILCT |
| H-1 → L | 0.1059 | ILCT | | | |
| H → L | 0.1497 | MLCT | | | |

^a Only the selected low-lying excited states are presented.

^b Oscillator strength.

^c H stands for HOMO and L stands for LUMO. Only the main configurations are presented.

^d The CI coefficients are in absolute values.

^e No spin-orbital coupling effect was considered, thus the f values are zero.

and LUMO of complex **Pt-3** was reduced to 3.51 eV, vs. the 3.84 eV of *ppyPt(acac)* (see Supporting information).

Compared to *ppyPt(acac)*, the contribution of Pt(II) ion to the HOMO and LUMO are significantly reduced in complex **Pt-3** (see Supporting information for the MOs of *ppyPt(acac)*). Thus we propose the ³IL is more prominent in the emissive state (mixed ³MLCT and ³LC) and the phosphorescent lifetime of the Pt complexes is expected to be longer [31]. This is fully supported by the experimental results that phosphorescent lifetime of 12.4 μs was observed for **Pt-3**, vs. lifetime of 2.6 μs for *ppyPt(acac)* [31].

The electronic structure of the low-lying electronic transitions were studied with the TDDFT method, based on the optimized

ground state geometries (Table 2). The calculated excitation energies are 409 nm, 383 nm, 336 nm, etc. These values are in good agreement with the experimental result of the UV–vis absorption spectra, which show absorption at 400 nm, 350 nm, 328 nm, etc (Fig. 1). The T₁ state was also studied in order to reveal the emissive property of the complex. We found the main component of the T₁ state is the HOMO → LUMO transition. These results clearly demonstrated that the involvement of the carbazole moiety in the T₁ state of the complex, which is responsible for the different emission property compared to *ppyPt(acac)*. The calculated energy level of T₁ state is 502 nm, which is in line with the experimental results (540 nm). Thus the red-shifted emission of the complex **Pt-3** can be rationalized by

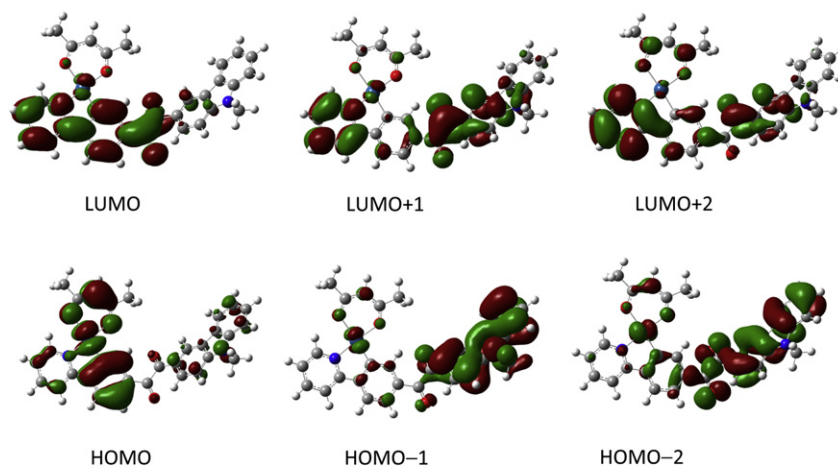


Fig. 4. Frontier molecular orbitals for **Pt-1**, calculated by DFT/TDDFT at the B3LYP/6-31G(d)/LanL2DZ level using Gaussian 09.

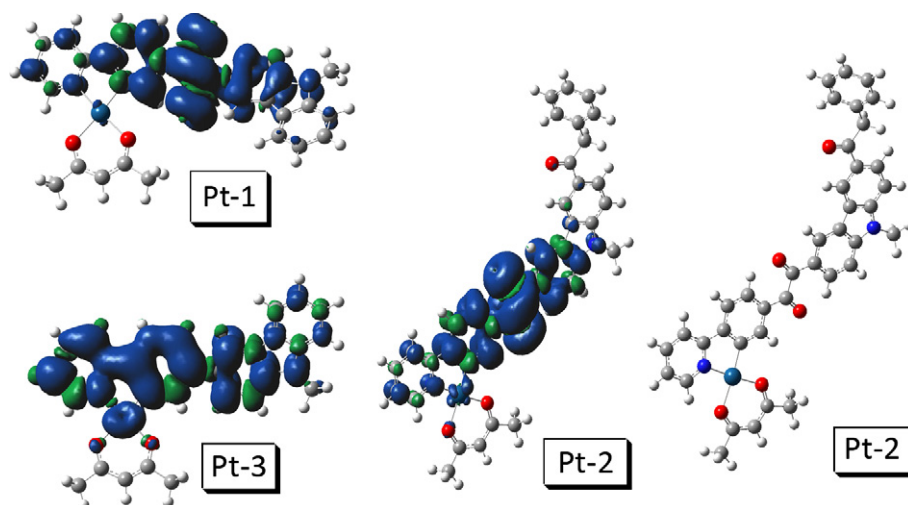


Fig. 5. Spin density surface of the complexes **Pt-1**, **Pt-2** and **Pt-3**. Calculated based on the optimized geometry of the lowest-lying triplet state. The molecular structure of **Pt-2** is presented for clarity.

attachment of the electron-donating carbazole moiety at the phenyl group of the *ppy* ligand (where HOMO is localized).

As close analogs to **Pt-3**, the α -diketo containing complexes **Pt-1** and **Pt-2** were also studied with the DFT/TDDFT calculations (Fig. 4 and Supporting information). The result indicates a *trans* skewed conformation for the α -diketo moiety [41], with torsion angle of 123.2° . However, both carbonyl groups take a coplanar geometry

with the *ppy* or the carbazole moiety to which it was attached, respectively. The optimized coordination angle O–Pt–O and C–Pt–N is 90.7° and 81.1° , respectively. The bond length of C–Pt and N–Pt is 1.98 Å and 2.02 Å, respectively. The optimized bond length O–Pt is in the range of 2.04 Å–2.15 Å. These values are close to the single crystal structures of the related cyclometalated Pt(II) (acac) complexes [34].

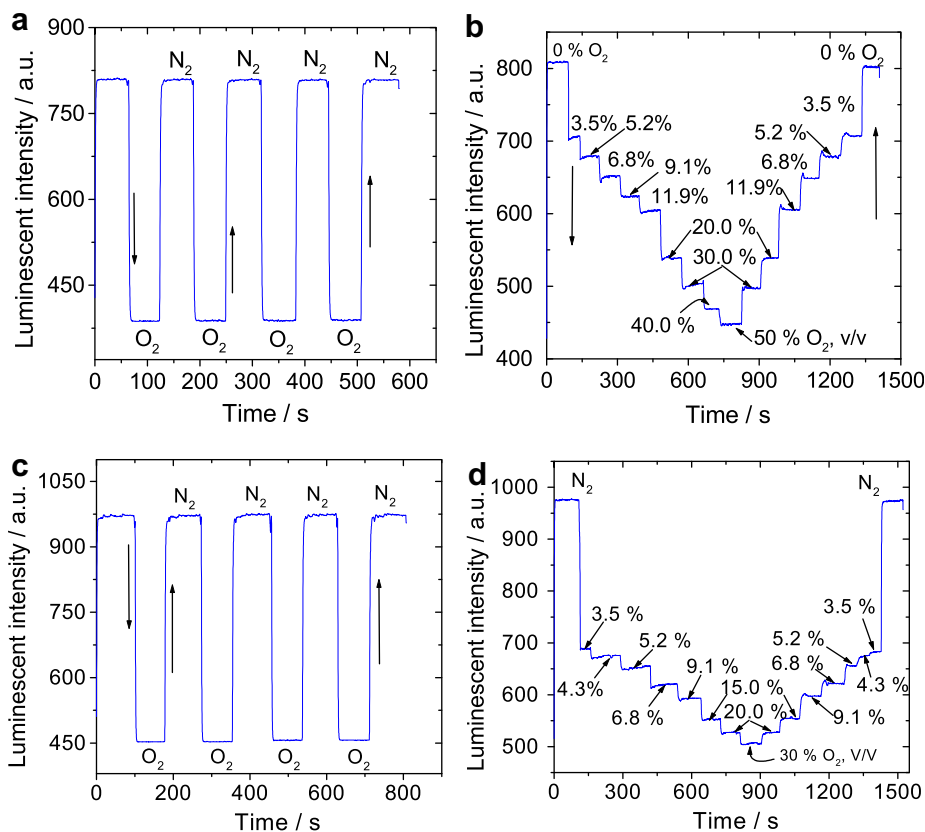


Fig. 6. Phosphorescent intensity response of sensing films of the complexes in IMPEK-C to step variations of O₂ concentrations. (a) response of complex **Pt-1** to switch between neat N₂ and O₂. $\lambda_{ex} = 370$ nm, $\lambda_{em} = 542$ nm. (b) dynamic response of complex **Pt-1** to variation of the oxygen concentrations of N₂/O₂ mixed gas. $\lambda_{ex} = 370$ nm, $\lambda_{em} = 542$ nm. (c) response of complex **Pt-3** to switch between neat N₂ and O₂. $\lambda_{ex} = 370$ nm, $\lambda_{em} = 536$ nm. (d) dynamic response of complex **Pt-3** to variation of the oxygen concentrations of N₂/O₂ mixed gas. $\lambda_{ex} = 370$ nm, $\lambda_{em} = 536$ nm.

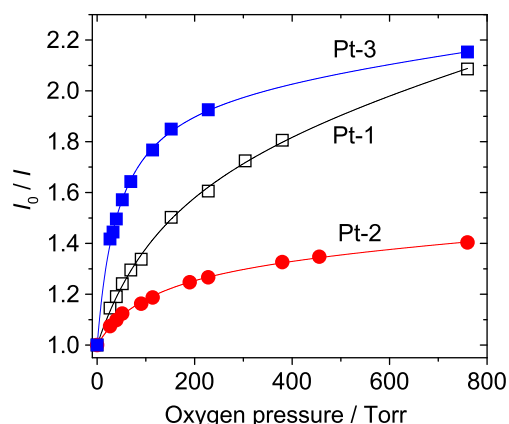


Fig. 7. Oxygen sensitivity of the emission of the complexes **Pt-1**, **Pt-2** and **Pt-3**. The fitting according to Eq. (2) of the oxygen sensing data in Fig. 6 and Fig. S30 in Supporting information.

For **Pt-1**, the first calculated absorption band is at 436 nm (S_2 state, with much higher oscillator strength than the S_1 state). This absorption is assigned as the ${}^1\text{MLCT}/{}^1\text{IL}$ transition (phenyl \rightarrow pyridine and Pt \rightarrow *ppy* charge transfer), which is in good agreement with the experimental results in the UV–vis absorption spectra. Excitations to higher singlet states were also calculated (Table 3). Calculations indicated that carbazole was involved in the transitions. It should be pointed that the α -diketo moiety was involved in the LUMO, this result infers that the diketo may act as electron trap (strong electron acceptor). Basically the excitation energies are consistent with the UV–vis absorption spectra (Fig. 1).

LUMO+1 and LUMO+2 were involved in these excitations and the diketo serves as electron trap in these molecular orbitals (Fig. 4). We noticed that S_1 state is featured with smaller f value than the S_2 state. This is probably due to the charge transfer feature of the S_1 state (carbazole \rightarrow *ppy*) [42].

In order to study the emissive state of the complex, the T_1 state is investigated with the TDDFT calculations and the electronic structure of T_1 state is listed in Table 3. carbazole \rightarrow *ppy* and Pt \rightarrow *ppy* charge transfer are involved in the T_1 state, thus the T_1 state can be described as ${}^3\text{MLCT}/{}^3\text{IL}$ mixed state. α -diketo moiety was involved in the orbitals such as LUMO, LUMO + 1 and LUMO + 3, which are involved in the T_1 state. Therefore, we conclude that α -diketone acts as electron sink and the emissive state of the complex **Pt-1** is different from the typical *ppyPt(acac)* complexes. The calculated energy level of T_1 state (545 nm) is close to the experimental results (554 nm).

Based on the frontier molecular orbitals, we found the α -diketo moiety is involved in the LUMO. The α -diketo moiety is electron deficient thus we expect the energy level will be decreased but the HOMO is nearly unaffected. Therefore we expected red-shifted emission wavelength for **Pt-1** than that of *ppyPt(acac)*. The DFT calculations indicate the energy levels of HOMO and LUMO of **Pt-1**

is -5.55 eV and -2.12 eV, respectively. Thus the energy gap between the HOMO and LUMO is $\Delta E_{\text{HOMO-LUMO}} = 3.43$ eV, by comparison *ppyPt(acac)* of -5.42 eV and -1.58 eV, respectively ($\Delta E_{\text{HOMO-LUMO}} = 3.84$ eV). Thus the red-shifted emission of the **Pt-1** can be rationalized by the electron sink effect of the α -diketo moiety, by which the energy level of the LUMO of the complex is decreased, but the energy level of the HOMO orbit is almost unaffected, a decreased HOMO-LUMO energy gap is obtained.

In order to study the phosphorescence origin of the complexes, the spin density surfaces of the triplet excited states of the complexes were investigated (Fig. 5). For **Pt-1** and **Pt-2**, the spin density is mainly localized in the 1,2-dione moieties. For **Pt-3**, however, the spin density is localized on the *ppy* ligand and the Pt center. Drastically different spin density distribution of the **Pt-1**, **Pt-2** and **Pt-3** indicate different photophysical properties of these complexes. These theoretical predictions are in agreement with the experimental results, which indicate similar phosphorescence lifetimes and phosphorescence quantum yields for **Pt-1** and **Pt-2**, but different photophysical properties for **Pt-3** (Table 1).

Our results show that the photophysical properties of the cyclometalated Pt complexes, such as the UV–vis absorption, can be studied with the DFT/TDDFT calculations. Our theoretical revealing the photophysics of the metalated Pt complexes may prove useful for future design of the cyclometalated Pt complexes with red-shifted emission compared to *ppyPt(acac)*.

2.5. Luminescent oxygen sensing properties of the cyclometalated Pt complexes

We have demonstrated that the complexes show phosphorescence with lifetimes in the range of μs (Table 1), which ensure efficient quenching of the emission by O_2 [1,2,20–25].

First we compared the response of the emission of the complexes **Pt-1**, **Pt-2** and **Pt-3** in solution to the variation of the O_2 partial pressure (See Supporting information). For **Pt-1**, the emission intensity is quenched by ca. 78.7% in air compared to the emission under N_2 . In O_2 , the emission intensity was quenched by 95.2% of the initial value that under N_2 (see Supporting information).

Pt-3 was also studied under similar condition (see Supporting information). We found the emission at 540 nm is highly sensitive to O_2 . The emission was almost completely quenched in air (ca. 21% O_2 v/v). Thus we propose the phosphorescence lifetime of **Pt-3** is much longer than that of **Pt-1** (Table 1), which is supported by the experimental result that a lifetime of 12.4 μs was observed for **Pt-3**, vs. the much shorter lifetime of 1.86 μs for **Pt-1**.

Stern–Volmer quenching equation (Eq. (1)) can be used to quantitatively describe the luminescence O_2 sensing. Where I_0 stands for emission intensity in inert atmosphere, I is the emission intensity under specific O_2 partial pressure, k_q is the quenching constant, τ_0 is the unquenched lifetime and $[Q]$ is the concentration of quencher. The longer the triplet excited state lifetime of a dye, the more sensitive of its emission to O_2 .

Table 4

Parameters of O_2 sensing film of complexes **Pt-1**, **Pt-2** and **Pt-3** with IMPEK-C as supporting matrix (fitting result of the two-site model).

| | f_1^a | f_2^a | $K_{\text{SV1}}^b/\text{Torr}^{-1}$ | $K_{\text{SV2}}^b/\text{Torr}^{-1}$ | r^{2c} | $K_{\text{SV}}^{\text{app}d}/\text{Torr}^{-1}$ | $p\text{O}_2^e/\text{Torr}$ |
|-------------|---------|---------|-------------------------------------|-------------------------------------|----------|--|-----------------------------|
| Pt-1 | 0.493 | 0.507 | 0.012 | 0.0002 | 0.9992 | 0.0058 | 86.9 |
| Pt-2 | 0.271 | 0.729 | 0.012 | 0.0001 | 0.9989 | 0.0032 | 86.2 |
| Pt-3 | 0.512 | 0.488 | 0.047 | 0.0001 | 0.9993 | 0.0238 | 21.5 |

^a The ratio of the two portion of the dyes.

^b The quenching constants of the two portions.

^c The determination coefficients.

^d Weighted quenching constant, $K_{\text{SV}}^{\text{app}} = f_1 \times K_{\text{SV1}} + f_2 \times K_{\text{SV2}}$.

^e The oxygen partial pressure at which the initial emission intensity of film is quenched by 50%, and can be calculated as $1/K_{\text{SV}}$.

$$\frac{I_0}{I} = 1 + k_q \tau_0 [Q] \quad (1)$$

For the heterogeneous O₂ sensing films, however, modified Stern–Volmer or two-site model is required to study the quenching effect [7–10], because even in “homogenous” polymers, the dye molecules still dwell in different microenvironments. In the two-site model, the O₂-responsive dyes are treated as two different portions. Fraction of the two portions are defined as *f*₁ and *f*₂, respectively (*f*₁ + *f*₂ = 1), the two portions show different quenching constants (*K*_{SV1} and *K*_{SV2}, Eq. (2)).

$$\frac{I_0}{I} = \frac{1}{\frac{f_1}{1 + K_{SV1} p_{O_2}} + \frac{f_2}{1 + K_{SV2} p_{O_2}}} \quad (2)$$

For practical O₂ sensor, the O₂ sensing property should be studied in solid matrix, such as polymer, or inorganic porous material [1,2]. The supporting matrix should ensure a fast response time (*t*_{↓95}, the time that elapsed before 95% of luminescence intensity change finished after switching the gas from N₂ to O₂) and recovery time (*t*_{↑95}, the time elapsed before 95% of luminescence intensity change finished after switching the gas from O₂ to N₂) [20–25]. Usually porous materials, such as MCM-41, are required to achieve a fast response vs. the variation of the O₂ partial pressures (concentration) [43,44]. Recently we found a specially designed aromatic polymer, IMPEK-C, with high oxygen permeability and diffusion coefficients, which is ideal for luminescent O₂ sensing matrix [20–25]. Therefore, the O₂ sensing properties of **Pt-1** and **Pt-3** were studied in the polymer film of IMPEK-C [45]. The films were prepared by the dissolution-casting method.

Firstly the O₂ sensing films were tested against O₂ and N₂ saturation cycles (Fig. 6a and c). The response time is as short as 3.3 s, and the recovery time is as short as 3.7 s [20,21]. Such fast response and recovery time are adequate for most applications. Fast response can usually be achieved with porous materials, such as MCM-41 [43,44,46–48]. Our solution-casting approach is straight forward (see experimental for oxygen sensing films preparation), thus can be used to easily fabricate reliable luminescent oxygen sensors.

Next, we examined the dynamic response of the sensing films of **Pt-1** and **Pt-3** vs. small steps variation of the O₂ partial pressure. Using this kind of test and the numeric fitting of the response with the two-site model, the O₂ sensing property of the complexes can be compared quantitatively. **Pt-3** is more sensitive to O₂ (Fig. 6d). With 3.5% O₂ (v/v), the emission intensity was quenched by 54.6%. Under the same condition, the sensing film of **Pt-1** only shows 24.8% quenching (Fig. 6b). Furthermore, the reversibility of the phosphorescence response in Fig. 6 demonstrated the good photostabilities of the complexes and the sensing films.

The sensing data were fitted with two-site model (Eq. (2)) (Fig. 7). The *K*_{SV} value of **Pt-3** is much higher than that of **Pt-1** and **Pt-2** (Table 4). We noticed the *K*_{SV} of **Pt-3** is 6.8-fold of a recently reported cyclometalated Ir(III) complex (*τ* = 4.3 μs in inert atmosphere) with diphenylamine capped *ppy* ligand (it should be pointed out that the supporting matrix for the Ir complex is ethyl cellulose) [11]. However, the *K*_{SV} values of the Pt(II) complexes described herein are lower than the metalloporphyrins, such as PtOEP, complexes with much longer lifetimes (>50 μs) [21].

3. Summary

Carbazole capped *ppy*Pt(acac) complexes with linkers of α -diketo (**Pt-1** and **Pt-2**) and C–C single bond (**Pt-3**) between the carbazole and the *ppy* group were synthesized and the

photophysical properties of the complexes were studied with experimental and theoretical methods. Oxidation of the ethynyl bond to α -diketo or methylene-keto structure were found for the metalation of the ethynyl ligands with K₂PtCl₄. Red-shifted emissions were observed for both the complexes with electron-donating (**Pt-3**) and electron-withdrawal groups (**Pt-1** and **Pt-2**) attached to *ppy*. **Pt-3** gives intensive room temperature phosphorescence with emission band at ca. 540 nm (Φ_p = 0.66) and prolonged phosphorescence lifetime (τ_p = 12.4 μs) compared to the model complex *ppy*Pt(acac) (λ_{em} = 486 nm, Φ_p = 0.15, τ_p = 2.6 μs). Based on the DFT calculations, we propose the red-shifted emission of **Pt-3** is due to the increased energy level of the HOMO, whereas the α -diketo is involved in the LUMO of **Pt-1** and **Pt-2** and as a result the energy level of LUMO is decreased. In both cases the energy gap between the HOMO and the LUMO is decreased compared to the model complex *ppy*Pt(acac). Thus the emissive states of **Pt-1** and **Pt-2** are different from the typical ³MLCT/³IL (Pt → *ppy* and phenyl → pyridine) of the normal *ppy*Pt(acac) complexes. The complexes were used for luminescent oxygen sensing. **Pt-3** shows the highest quenching constant (*K*_{SV} = 0.0238 Torr⁻¹), which is 6.8-fold of a reported cyclometalated Ir(III) complex used for luminescent oxygen sensing.

4. Experimental

4.1. General procedures, materials and physical measurements

The general procedure for the preparation is given in Scheme 1. All the chemicals are analytical pure and were used as received without further purification. NMR spectra were taken on a 400 MHz Varian Unity Inova spectrophotometer. Mass spectra were recorded with Q-TOF Micro MS spectrometer. UV–vis spectra were taken on an HP8453 UV–visible spectrophotometer. Fluorescence spectra were recorded on a JASCO FP-6500 or a Sanco 970 CRT spectrofluorometer. Phosphorescence quantum yields were measured with complex Pt(^tBu₂bpy)(C≡C–Ph)₂ (Φ = 0.496 in MeCN) as the reference [49]. Luminescence lifetimes were measured on a Horiba Jobin Yvon Fluoro Max-4 (TCSPC) instrument.

The structures of the complexes were optimized using density functional theory (DFT) with B3LYP functional and 6-31G(d)/LanL2DZ basis set. 6-31G(d) basis set were employed for C, H, N, O and LanL2DZ basis set was used for Pt(II). The excited state related calculations were carried out with the time dependent DFT (TDDFT) based on the optimized ground state geometry. The spin density surfaces of the complexes were calculated based on the optimized geometry of the T₁ excited states. All these calculations were performed with Gaussian 09 [50].

4.2. Synthesis

4.2.1. 9-Butyl-3-iodocarbazole (2)

n-C₄H₉Br (1.48 mL, 13.8 mmol) were added to a solution of compound **1** (4.0 g, 13.7 mmol) in DMF (30 mL). Then, NaH (70 wt.% in mineral oil, 960.0 mg, 28 mmol) was added in portions. The mixture was stirred at room temperature until the reaction was completed (monitored by TLC). The reaction mixture was poured into water (200 mL), the precipitate was collected by filtration, and purified with column chromatography (silica gel, petroleum ether:DCM = 1:1, v/v) to give 3.52 g white solid. Yield: 73.8%. ¹H NMR (400 MHz, CDCl₃): 8.40 (s, 1H), 8.04 (d, 1H, *J* = 7.6 Hz), 7.71 (d, 1H, *J* = 10.1 Hz), 7.51 (t, 1H, *J* = 7.3 Hz), 7.41 (d, 1H, *J* = 8.2 Hz), 7.24 (t, 1H, *J* = 7.3 Hz), 7.20 (d, 1H, *J* = 8.4 Hz), 4.26 (t, 2H, *J* = 7.3 Hz), 1.87–1.80 (m, 2H), 1.43–1.33 (m, 2H), 0.94 (t, 3H, *J* = 7.3 Hz).

4.2.2. 9-Butyl-3-ethynylcarbazole (**3**)

Under Ar atmosphere, compound **2** (2.8 g, 8.0 mmol), Pd(PPh₃)₂Cl₂ (103.2 mg, 0.16 mmol), PPh₃ (83.0 mg, 0.3 mmol), CuI (15.2 mg, 0.08 mmol) were dissolved in NEt₃ (30 mL). After stirring for 5 min, ethynyltrimethylsilane (1.4 mL, 9.6 mmol) was added via syringe. The solution was refluxed for 8 h. The solvent was removed under reduced pressure and the crude product was purified by column chromatography (silica gel, dichloromethane/petroleum ether = 1:4, v/v), brown solid was obtained. The above trimethylsilane protected intermediate was dissolved in methanol (30 mL), K₂CO₃ (1.2 g) was added and the mixture was stirred at r.t. for 3 h. The solvent was removed under reduced pressure. Water was added and the mixture was extracted with CH₂Cl₂. The organic layer was dried over anhydrous Na₂SO₄. After removal of the solvent, compound **3** was obtained as light yellow solid. 620.0 mg, yield: 34.0%. ¹H NMR (400 MHz, CDCl₃) 8.24 (s, 1H), 8.04 (d, 1H, *J* = 7.8 Hz), 7.57 (d, 2H, *J* = 8.4 Hz), 7.44 (t, 1H, *J* = 7.8 Hz), 7.36 (d, 1H, *J* = 8.1 Hz), 7.28 (d, 1H, *J* = 8.4 Hz), 7.23–7.19 (m, 1H), 4.20 (t, 2H, *J* = 7.2 Hz), 3.05 (s, 1H), 1.82–1.74 (m, 2H), 1.38–1.29 (m, 2H), 0.90 (t, 3H, *J* = 7.3 Hz).

4.2.3. 2-(4-Bromophenyl) pyridine (**4**)

At 0 °C, an aqueous solution of NaNO₂ (4.14 g, 0.06 mmol, 7.5 mL of 8.0 M solution, 2 equivalent) was slowly added to a suspension of *p*-bromoaniline (5.00 g, 30 mmol, 1 equivalent) in concentrated HCl (10 mL). The mixture was stirred at 0 °C for 1 h and was carefully added into pyridine (125 mL) by dropwise. The brown solution was stirred at 40 °C for 4 h and then Na₂CO₃ (50.0 g) was added and the slurry was stirred for 18 h. The reaction mixture was extracted with CH₂Cl₂ (3 × 50 mL) and the combined organic layers were dried over anhydrous Na₂SO₄ and evaporated to dryness. The crude product was purified with column chromatography (silica gel, CH₂Cl₂ as the eluent). Orange solid was obtained, 2.58 g, yield: 37.0%. ¹H NMR (400 MHz, CDCl₃) 8.68 (d, 1H, *J* = 4.0 Hz), 7.86 (d, 2H, *J* = 8.4 Hz), 7.77 (t, 2H, *J* = 6.4 Hz), 7.73 (d, 1H, *J* = 8.4 Hz), 7.58 (d, 2H, *J* = 8.4 Hz), 7.25 (t, 1H, *J* = 6.0 Hz).

4.2.4. Ligand **L1**

Under argon atmosphere, compound **3** (380.0 mg, 1.54 mmol) and **4** (360.0 mg, 1.54 mmol) were dissolved in mixed solvent of toluene (8 mL) and (*i*-Pr)₂NH (8 mL). Then Pd(PPh₃)₄ (71.9 mg, 0.06 mmol), CuI (24.6 mg, 0.12 mmol) were added, the mixture was refluxed for ca. 8 h. The reaction mixture was cooled to r.t. and the solvent was removed under reduced pressure. Water was added and the mixture was extracted with CH₂Cl₂. The organic layer was dried over anhydrous Na₂SO₄. After removal of the solvent, the crude product was purified with column chromatography (silica gel, CH₂Cl₂:hexane = 1:1, v/v). Orange solid was obtained (250.0 mg), yield: 40.5%. ¹H NMR (400 MHz, CDCl₃) : 8.74 (d, 1H, *J* = 4.6 Hz), 8.33 (s, 1H), 8.12 (d, 1H, *J* = 7.9 Hz), 8.05 (d, 2H, *J* = 8.1 Hz), 7.82 (t, 2H, *J* = 7.6 Hz), 7.70–7.65 (m, 3H), 7.52 (t, 1H, *J* = 8.0 Hz), 7.44–7.38 (m, 2H), 7.29–7.26 (m, 2H), 4.34 (t, 2H, *J* = 7.1 Hz), 1.91–1.84 (m, 2H), 1.46–1.37 (m, 2H), 0.98 (t, 3H, *J* = 7.3 Hz). ¹³C NMR (100 MHz, CDCl₃) δ 156.79, 149.83, 140.96, 140.33, 138.49, 137.08, 132.00, 129.44, 126.94, 126.26, 124.79, 124.28, 123.01, 122.60, 122.45, 120.73, 120.70, 119.51, 113.18, 109.11, 108.94, 92.51, 87.67, 43.15, 31.27, 20.73, 14.06. HRMS ([C₂₉H₂₄N₂ + H]⁺) calcd 401.2018, found 401.2020.

4.2.5. Complex **Pt-1**

Compound **L1** (233.0 mg, 0.582 mmol) was dissolved in mixed solvent of 2-ethoxyethanol (15.0 mL) and water (5 mL), then K₂PtCl₄ (120.8 mg, 0.29 mmol) was added, the mixture was heated to 80 °C for 16 h under argon atmosphere. After cooling to r.t., the reaction mixture was poured into water (20 mL) and the precipitate was washed with water (4 × 20 mL) and dried under vacuum. The

precipitate was used to react with Hacac (43.7 mg, 0.437 mmol) in the presence of Na₂CO₃ (154.2 mg, 0.437 mmol) in 2-ethoxyethanol (16 mL) at 100 °C for 16 h. The reaction mixture was then poured into water, the precipitate was purified with column chromatography (silica gel, eluting with CH₂Cl₂) to afford the product as yellow solid (50.0 mg), yield: 24.8%. ¹H NMR (400 MHz, CDCl₃) : 9.04 (d, 1H, *J* = 5.7 Hz), 8.73 (s, 1H), 8.28 (s, 1H), 8.14 (t, 2H, *J* = 8.7 Hz), 7.87 (t, 1H, *J* = 7.7 Hz), 7.75 (d, 1H, *J* = 7.9 Hz), 7.68 (d, 1H, *J* = 8.0 Hz), 7.52–7.49 (m, 2H), 7.45 (d, 2H, *J* = 7.5 Hz), 7.31 (d, 1H, *J* = 7.5 Hz), 7.22 (t, 1H, *J* = 6.1 Hz), 5.44 (s, 1H), 4.35 (t, 2H, *J* = 7.1 Hz), 2.00 (s, 3H), 1.91 (s, 3H), 1.88–1.82 (m, 2H), 1.44–1.34 (m, 2H), 0.96 (t, 3H, *J* = 7.3 Hz). ¹³C NMR (100 MHz, CDCl₃) δ 196.79, 195.27, 186.07, 184.73, 184.65, 166.86, 150.94, 147.99, 144.33, 141.44, 139.70, 138.58, 133.12, 131.87, 127.83, 126.90, 125.86, 125.12, 124.03, 123.36, 122.99, 121.20, 120.60, 119.88, 109.55, 109.10, 102.73, 43.39, 31.25, 29.90, 28.36, 27.16, 20.70, 14.01. MALDI-HRMS ([C₃₄H₃₀N₂O₄Pt]⁻) calcd 725.1853, found 725.1911.

4.2.6. 3-Bromo-9-butyl-6-iodocarbazole (**5**)

Under argon atmosphere, the solution of *N*-bromosuccinimide (NBS) (1.02 g, 5.73 mmol) in 6.0 mL DMF was added dropwise to a solution of compound **2** (2.0 g, 5.73 mmol) in DMF (6 mL). The mixture was heated at 60 °C for 6 h and then cooled to r.t., the reaction mixture was then poured into water, and the precipitate was collected, washed with water and dried. Pale solid (1.20 g) was obtained, yield: 44.7%. ¹H NMR (400 MHz, CDCl₃): 8.33 (d, 1H, *J* = 1.3 Hz), 8.13 (d, 1H, *J* = 1.5 Hz), 7.72–7.69 (m, 1H, *J* = 8.6 Hz), 7.56–7.53 (m, 1H, *J* = 8.7 Hz), 7.27 (t, 1H, *J* = 4.7 Hz), 7.19 (t, 1H, *J* = 8.5 Hz), 4.25 (t, 2H, *J* = 7.1 Hz), 1.84–1.76 (m, 2H), 1.37–1.31 (m, 2H), 0.94 (t, 3H, *J* = 7.3 Hz).

4.2.7. 3-Bromo-9-butyl-6-phenylethynylcarbazole (**6**)

Under argon atmosphere, compound **5** (1.13 g, 2.64 mmol) was dissolved in mixed solvent of dry toluene (10 mL) and (*i*-Pr)₂NH (8 mL), Pd(PPh₃)₄ (92.0 mg, 0.08 mmol), CuI (10.0 mg, 0.05 mmol) were added, then phenylethyne (270.0 mg, 2.64 mmol) was added via syringe. The mixture was refluxed for 2 h. The reaction mixture was then cooled to r.t. and the solvent was removed under reduced pressure. The crude product was purified with column chromatography (silica gel, CH₂Cl₂:hexane = 1:5, v/v) and a light yellow oily liquid was obtained, 950.0 mg, yield: 90.0%. ¹H NMR (400 MHz, CDCl₃): 8.24 (d, 1H, *J* = 1.0 Hz), 8.20 (d, 1H, *J* = 1.7 Hz), 7.67 (q, 1H, *J* = 8.5 Hz), 7.59–7.54 (m, 3H), 7.30 (d, 1H, *J* = 8.8 Hz), 4.29 (t, 2H, *J* = 7.3 Hz), 1.88–1.80 (m, 2H), 1.43–1.33 (m, 2H), 0.97 (t, 3H, *J* = 7.3 Hz).

4.2.8. 9-Butyl-3-ethynyl-6-phenylethynylcarbazole (**7**)

Under argon atmosphere, compound **6** (0.90 g, 2.23 mmol), Pd(PPh₃)₄ (104.1 mg, 0.09 mmol), CuI (34.0 mg, 0.18 mmol) were dissolved in NEt₃ (15 mL). After stirring, ethynyltrimethylsilane (306.8 mg, 3.12 mmol) was added via syringe. The solution was refluxed for 8 h. The solvent was removed under reduced pressure and the crude product was purified by column chromatography (silica gel, dichloromethane/petroleum ether = 1:5, v/v), yellow oil (600 mg, 1.43 mmol) was obtained, yield: 64.1%. The above trimethylsilane protected intermediate was dissolved in methanol (20 mL), K₂CO₃ (800 mg, 7.55 mmol) was added and the mixture was stirred at r.t. for 3 h. The solvent was removed under reduced pressure. Water was added and the mixture was extracted with CH₂Cl₂. The organic layer was dried over anhydrous Na₂SO₄. After removal of the solvent, compound **3** was obtained. 470.0 mg, yield: 94.8%. ¹H NMR (400 MHz, CDCl₃): 8.26 (d, 2H, *J* = 7.0 Hz), 7.66–7.57 (m, 4H), 7.38–7.33 (m, 5H), 4.31 (t, 2H, *J* = 7.2 Hz), 3.09 (s, 1H), 1.89–1.81 (m, 2H), 1.44–1.34 (m, 2H), 0.97 (t, 3H, *J* = 7.2 Hz).

4.2.9. Ligand **L2**

Under argon atmosphere, compound **7** (440.0 mg, 1.27 mmol) and compound **4** (397.3 mg, 1.27 mmol) were dissolved in mixed solvent of toluene (7 mL) and (i-Pr)₂NH (7 mL). Then Pd(PPh₃)₄ (59.3 mg, 0.05 mmol), CuI (19.3 mg, 0.10 mmol) were added, the mixture was refluxed for 8 h. The reaction mixture was cooled to r.t. and the solvent was removed under reduced pressure. Water was added and the mixture was extracted with CH₂Cl₂. The organic layer was dried over anhydrous Na₂SO₄. After removal of the solvent the crude product was purified with column chromatography (silica gel, dichloromethane:hexane = 1:1). Orange solid (274.1 mg, 0.505 mmol) was obtained, yield 40.0%. ¹H NMR (400 MHz, CDCl₃): 8.73 (d, 1H, *J* = 4.8 Hz), 8.30 (d, 2H, *J* = 5.3 Hz), 8.04 (d, 2H, *J* = 8.1 Hz), 7.80 (d, 2H, *J* = 12.3 Hz), 7.70–7.65 (m, 4H), 7.60 (d, 2H, *J* = 7.2 Hz), 7.39–7.31 (m, 5H), 7.27–7.24 (m, 1H), 4.32 (t, 2H, *J* = 7.1 Hz), 1.90–1.83 (m, 2H), 1.45–1.36 (m, 2H), 0.98 (t, 3H, *J* = 7.4 Hz). ¹³C NMR (100 MHz, CDCl₃) δ 156.76, 149.74, 140.73, 140.67, 138.48, 137.22, 137.15, 132.07, 131.69, 129.94, 128.51, 128.02, 127.00, 124.84, 124.42, 124.36, 124.07, 122.73, 122.51, 122.45, 120.81, 120.75, 114.20, 114.13, 114.03, 109.20, 92.31, 90.78, 88.06, 88.03, 43.32, 31.26, 20.68, 13.98. HRMS ([C₃₇H₂₈N₂ + H]⁺) calcd 501.2335, found 501.2331.

4.2.10. Complex **Pt-2**

Compound **Pt-2** was obtained following a similar procedure outlined above for **Pt-1**, except the ligand **L2** (300.0 mg, 0.599 mmol) was used instead of **L1**, yield: 15 mg, 6.3%. ¹H NMR (400 MHz, acetone): 9.15 (s, 1H), 8.95 (d, 1H, *J* = 5.8 Hz), 8.90 (s, 1H), 8.19–8.12 (m, 3H), 7.70–7.67 (m, 1H), 7.95 (d, 1H, *J* = 7.7 Hz), 7.80 (d, 1H, *J* = 8.7 Hz), 7.72–7.65 (m, 3H), 7.37–7.31 (m, 3H), 7.24 (t, 2H, *J* = 7.3 Hz), 7.17–7.13 (m, 1H), 5.47 (s, 1H), 4.49 (t, 2H, *J* = 7.0 Hz), 4.42 (s, 2H), 1.92 (s, 3H), 1.86–1.82 (m, 2H), 1.78 (s, 3H), 1.38–1.30 (m, 2H), 0.87 (t, 3H, *J* = 7.3 Hz). ¹³C NMR (100 MHz, acetone-d₆) δ 196.53, 196.38, 195.38, 186.31, 184.00, 166.14, 151.35, 147.70, 145.05, 144.15, 140.13, 139.46, 136.10, 132.58, 131.45, 129.87, 129.39, 128.45, 127.84, 127.73, 127.58, 127.50, 127.42, 126.52, 125.89, 125.04, 124.02, 123.74, 123.48, 123.39, 123.07, 122.75, 120.52, 110.60, 110.13, 102.30, 44.87, 43.24, 31.11, 27.50, 26.35, 20.23, 13.39. MALDI-MS ([C₄₂H₃₆N₂O₅Pt]⁻) calcd 843.2272, found 843.0262.

4.2.11. Ligand **L3**

Under Ar atmosphere, compound **4** (400 mg, 1.71 mmol) was added to anhydrous THF (5.0 mL) in a Schlenk flask at -78 °C. Then *n*-BuLi (2.5 M in hexane, 1.46 mL, 3.42 mmol) was added dropwise. The mixture was stirred at -78 °C for 45 min, after which a solution of anhydrous ZnCl₂ (466 mg, 3.42 mmol) in anhydrous THF (10 mL) was added slowly and the mixture was stirred for 1.5 h at room temperature. Then a solution of 9-butyl-3-iodo-9H-carbazole (596.4 mg, 1.71 mmol) and Pd(PPh₃)₄ (60.0 mg, 0.05 mmol) in THF (10 mL) was added, and the reaction mixture was refluxed under an argon atmosphere for 16 h. The mixture was cooled to r.t., a solution of NH₄Cl (2.0 g, 37 mmol) in water (10 mL) was added. Then the mixture was stirred for 15 min and was extracted with CH₂Cl₂ (3 × 20 mL), and dried over anhydrous Na₂SO₄. The crude product was purified with column chromatography (silica gel, CH₂Cl₂ as the eluent) and orange solid (100 mg) was obtained, yield 15.6%. ¹H NMR (400 MHz, CDCl₃): 8.72 (d, 1H, *J* = 4.8 Hz), 8.38 (s, 1H), 8.17 (d, 1H, *J* = 7.5 Hz), 8.12 (d, 2H, *J* = 8.0 Hz), 7.84 (d, 2H, *J* = 8.3 Hz), 7.79–7.94 (m, 3H), 7.50–7.41 (m, 3H), 7.29–7.20 (m, 2H), 4.33 (t, 2H, *J* = 7.3 Hz), 1.91–1.83 (m, 2H), 1.46–1.36 (m, 2H), 0.97 (t, 3H, *J* = 7.6 Hz). ¹³C NMR (100 MHz, CDCl₃) δ 157.22, 149.70, 142.70, 140.91, 140.12, 137.32, 136.73, 131.51, 127.48, 127.28, 125.83, 125.05, 123.38, 122.95, 121.94, 120.46, 120.37, 118.95, 118.82, 108.96, 108.88, 42.96, 31.16, 20.59, 13.91. HRMS ([C₂₇H₂₄N₂ + H]⁺) calcd 377.2030, found 377.2018.

4.2.12. Complex **Pt-3**

Compound **Pt-3** was obtained following a similar procedure outlined above for **Pt-1**, except the ligand **L3** (100.0 mg, 0.266 mmol) was used instead of **L1**, yield: 45.0 mg, 50.6%. ¹H NMR (400 MHz, CDCl₃): 9.01 (d, 1H, *J* = 5.8 Hz), 8.44 (s, 1H), 8.16 (d, 1H, *J* = 7.8 Hz), 7.95 (s, 1H), 7.85 (d, 1H, *J* = 8.5 Hz), 7.80 (t, 1H, *J* = 7.8 Hz), 7.64 (d, 1H, *J* = 8.1 Hz), 7.53 (d, 1H, *J* = 8.1 Hz), 7.48–7.41 (m, 4H), 7.24 (d, 1H, *J* = 7.3 Hz), 7.10 (t, 1H, *J* = 6.5 Hz), 5.49 (s, 1H), 4.35 (t, 2H, *J* = 7.0 Hz), 2.03 (s, 3H), 2.02 (s, 3H), 1.93–1.85 (m, 2H), 1.48–1.38 (m, 2H), 0.98 (t, 3H, *J* = 7.3 Hz). ¹³C NMR (100 MHz, CDCl₃) δ 185.72, 184.23, 168.24, 147.29, 142.99, 142.94, 140.92, 140.08, 139.07, 138.03, 132.88, 129.02, 125.64, 125.46, 123.39, 123.23, 123.15, 122.90, 120.77, 120.46, 119.12, 118.79, 118.27, 108.79, 108.73, 102.52, 42.98, 31.19, 29.71, 28.29, 27.28, 20.60, 13.90. MALDI-HRMS ([C₃₂H₃₀N₂O₄Pt]⁺) calcd 669.1955, found 669.1961.

4.2.13. Oxygen sensing films

Typical film preparation is as following. 10.0 mg of IMPEK-C polymer was dissolved in 0.5 mL chloroform, then 0.4 mL of cyclometalated platinum complexes solution in DCM (1.0 × 10⁻³ mol dm⁻³) was added into the solution. After thorough mixing, about 0.25 mL of the solution was coated on a silica glass disk (diameter: 1.6 cm). The solvent was evaporated at r.t. and a transparent film was obtained. The thickness of the film of complex **Pt-1** was estimated as 12.7 mm, by the weight of the film (2.9 mg) and the density of the polymer (1.14 g cm⁻³). The thickness of the film of **Pt-2** and **Pt-3** was estimated with the same method as 13.2 mm and 11.8 mm, respectively.

Acknowledgment

We thank the NSFC (20972024 and 21073028), the Fundamental Research Funds for the Central Universities (DUT10ZD212), Ministry of Education (SRFDP-200801410004 and NCET-08-0077), the Royal Society (UK) and NSFC (China-UK Cost-Share Science Networks, 21011130154), PCSIRT (IRT0711), the Education Department of Liaoning Province (2009T015), State Key Laboratory of Fine Chemicals (KF0802) and Dalian University of Technology for financial support

Appendix. Supporting information

Supplementary data related to this article can be found online at doi:10.1016/j.jorganchem.2011.03.002.

References

- W.Y. Wong, J. Organomet. Chem. 694 (2009) 2644–2647.
- C.L. Ho, W.Y. Wong, Z.Q. Gao, C.H. Chen, K.W. Cheah, B. Yao, Z. Xie, Q. Wang, D. Ma, L. Wang, X.M. Yu, H.S. Kwok, Z. Lin, Adv. Funct. Mater. 18 (2008) 319–331.
- C.M. Che, C.C. Kwok, S.W. Lai, A.F. Rausch, W.J. Finkenzeller, N. Zhu, H. Yersin, Chem. Eur. J. 16 (2010) 233–247.
- G.J. Zhou, Q. Wang, W.Y. Wong, D. Ma, L. Wang, Z. Lin, J. Mater. Chem. 19 (2009) 1872–1883.
- R. Narayanaswamy, O.S. Wolfbeis, Optical Sensors: Industrial, Environmental and Diagnostic Applications. Springer-Verlag, Berlin-Heidelberg, 2004.
- J.R. Lakowicz, Principles of Fluorescence Spectroscopy, second ed. Kluwer Academic, New York, 1999.
- E.R. Carraway, J.N. Demas, B.A. DeGraff, J.R. Bacon, Anal. Chem. 63 (1991) 337–342.
- L. Sacksteder, J.N. Demas, B.A. DeGraff, J.R. Bacon, Anal. Chem. 65 (1993) 3480–3483.
- J.A.G. Williams, Top. Curr. Chem. 281 (2007) 205–268.
- R.A. Kirgan, B.P. Sullivan, D.P. Rillema, Top. Curr. Chem. 281 (2007) 143–203.
- C.S.K. Mak, D. Pentlechner, M. Stich, O.S. Wolfbeis, W.K. Chan, H. Yersin, Chem. Mater. 21 (2009) 2173–2175.
- G.D. Marco, M. Lanza, A. Mamo, I. Stefio, C.D. Pietro, G. Romeo, S. Campagna, Anal. Chem. 70 (1998) 5019–5023.
- M.C. DeRosa, P.J. Mosher, G.P.A. Yap, K.S. Focsaneanu, R.J. Crutchley, C.E.B. Evans, Inorg. Chem. 42 (2003) 4864–4872.
- M.C. DeRosa, D.J. Hodgson, G.D. Enright, B. Dawson, C.E.B. Evans, R.J. Crutchley, J. Am. Chem. Soc. 126 (2004) 7619–7626.

- [15] S.M. Borisov, I. Klimant, *Anal. Chem.* 79 (2007) 7501–7509.
- [16] W. Xu, K.A. Kneas, J.N. Demas, B.A. DeGraff, *Anal. Chem.* 68 (1996) 2605–2609.
- [17] Y. Wang, B. Li, Y. Liu, L. Zhang, Q. Zuo, L. Shi, Z. Su, *Chem. Commun.* (2009) 5868–5870.
- [18] E.V. Donckt, B. Camerman, R. Herne, R. Vandeloise, *Sens. Actuators B* 32 (1996) 121–127.
- [19] K.A. Kneas, W. Xu, J.N. Demas, B.A. DeGraff, A.P. Zipp, *J. Fluoresc.* 8 (1998) 295–300.
- [20] S. Ji, W. Wu, W. Wu, P. Song, K. Han, Z. Wang, S. Liu, H. Guo, J. Zhao, *J. Mater. Chem.* 20 (2010) 1953–1963.
- [21] S. Ji, W. Wu, Y. Wu, T. Zhao, F. Zhou, Y. Yang, X. Zhang, X. Liang, W. Wu, L. Chi, Z. Wang, J. Zhao, *Analyst* 134 (2009) 958–965.
- [22] W. Wu, W. Wu, S. Ji, H. Guo, J. Zhao, *Eur. J. Inorg. Chem.* 29 (2010) 4470–4482.
- [23] W. Wu, C. Cheng, W. Wu, H. Guo, S. Ji, P. Song, K. Han, J. Zhao, X. Zhang, Y. Wu, G. Du, *Eur. J. Inorg. Chem.* 29 (2010) 4683–4696.
- [24] W. Wu, S. Ji, W. Wu, H. Guo, X. Wang, J. Zhao, Z. Wang, *Sens. Actuators B* 149 (2010) 395–406.
- [25] S. Ji, H. Guo, X. Yuan, X. Li, H. Ding, P. Gao, C. Zhao, W. Wu, W. Wu, J. Zhao, *Org. Lett.* 12 (2010) 2876–2879.
- [26] X. Wang, A.D. Guerso, R.H.J. Schmehl, *Photochem. Photobiol. C* 5 (2004) 55–77.
- [27] N.D. McClenaghan, Y. Leydet, B. Maubert, M.T. Indelli, S. Campagna, *Coord. Chem. Rev.* 249 (2005) 1336–1350.
- [28] A.I. Baba, J.R. Shaw, J.A. Simon, R.P. Thummel, R.H. Schmehl, *Coord. Chem. Rev.* 171 (1998) 43–59.
- [29] H. Xiao, H. Shen, Y. Lin, J. Su, H. Tian, *Dyes Pigm.* 73 (2007) 224–229.
- [30] C. Mousset, A. Giraud, O. Provot, A. Hamze, J. Bignon, J. Liu, S. Thoret, J. Dubois, J. Brion, M. Alami, *Bioorg. Med. Chem. Lett.* 18 (2008) 3266–3271.
- [31] J. Brooks, Y. Babayan, S. Lamansky, P.I. Djurovich, I. Tsyba, R. Bau, M.E. Thompson, *Inorg. Chem.* 41 (2002) 3055–3066.
- [32] R.M. Adhikari, D.C. Neckers, *J. Org. Chem.* 74 (2009) 3341–3349.
- [33] Z. He, W.Y. Wong, X. Yu, H.S. Kwok, Z. Lin, *Inorg. Chem.* 45 (2006) 10922–10937.
- [34] J.F. Gong, X.H. Fan, C. Xu, J.L. Li, Y.J. Wu, M.P. Song, *J. Organomet. Chem.* 692 (2007) 2006–2013.
- [35] C. Yang, X. Zhang, H. You, L. Zhu, L. Chen, L. Zhu, Y. Tao, D. Ma, Z. Shuai, J. Qin, *Adv. Funct. Mater.* 17 (2007) 651–661.
- [36] F. Han, L. Chi, X. Liang, S. Ji, S. Liu, F. Zhou, Y. Wu, K. Han, J. Zhao, T.D. James, *J. Org. Chem.* 74 (2009) 1333–1336.
- [37] X. Zhang, L. Chi, S. Ji, Y. Wu, P. Song, K. Han, H. Guo, T.D. James, J. Zhao, *J. Am. Chem. Soc.* 131 (2009) 17452–17463.
- [38] A. Vlček Jr., S. Zális, *Coord. Chem. Rev.* 251 (2007) 258–287.
- [39] G.J. Zhao, J.Y. Liu, L.C. Zhou, K.L. Han, *J. Phys. Chem. B* 111 (2007) 8940–8945.
- [40] Z.D. Yang, J.K. Feng, A.M. Ren, *Inorg. Chem.* 47 (2008) 10841–10850.
- [41] M.R. Ams, D. Ajami, S.L. Craig, J.S. Yang, J. Rebek Jr., *J. Am. Chem. Soc.* 131 (2009) 13190–13191.
- [42] S. Ji, J. Yang, Q. Yang, S. Liu, M. Chen, J. Zhao, *J. Org. Chem.* 74 (2009) 4855–4865.
- [43] B. Wang, Y. Liu, B. Li, S. Yue, W. Li, *J. Lumin.* 128 (2008) 341–347.
- [44] H. Zhang, Y. Sun, K. Ye, P. Zhang, Y. Wang, *J. Mater. Chem.* 15 (2005) 3181–3186.
- [45] Z. Wang, T. Chen, J. Xu, *Macromolecules* 33 (2000) 5672–5679.
- [46] N. Leventis, A.M.M. Rawashdeh, I.A. Elder, J. Yang, A. Dass, C. Sotiriou-Leventis, *Chem. Mater.* 16 (2004) 1493–1506.
- [47] T.S. Yeh, C.S. Chu, Y.L. Lo, *Sens. Actuators B* 119 (2006) 701–707.
- [48] B.J. Basu, *Sens. Actuators B* 123 (2007) 568–577.
- [49] H. Guo, S. Ji, W. Wu, W. Wu, J. Shao, J. Zhao, *Analyst* 135 (2010) 2832–2840.
- [50] M.J. Frisch, G.W. Trucks, H.B. Schlegel, et al., *Gaussian 09 Revision A.1*. Gaussian Inc., Wallingford CT, 2009.